# Excitation Strategies for 3-D Electrical Capacitance Tomography Sensors

Jingjing Shen<sup>®</sup>, Shuanghe Meng<sup>®</sup>, Wuqiang Yang<sup>®</sup>, Fellow, IEEE, and Mao Ye<sup>®</sup>

Abstract—This article presents investigation of 3-D electrical capacitance tomography (ECT) sensors with different excitation strategies, including dual-electrode excitation in the same plane, in adjacent plane, in planes separated by one plane or two planes, and in the adjacent position or opposite position in the same or different planes. The results show that a 3-D ECT sensor with dual-electrode excitation in the opposite position provides higher mean capacitance and lower standard deviation than in the adjacent position. Dual-electrode excitation in different planes can increase the capacitance signal and decrease the dynamic range of capacitance measurements, and thus, decrease random errors and improve the quality of 3-D reconstructed images. A 3-D ECT sensor with dual-electrode excitation in planes separated by one plane and opposite position can provide small measurement uncertainty and high image quality.

Index Terms—3-D electrical capacitance tomography (ECT), excitation strategy, measured signal, image quality.

### I. INTRODUCTION

A FLOW in a gas-solid fluidized bed is complex and dynamically changing with time [1]. To maintain good operation of a gas-solid fluidized bed, the measurement technique used to obtain operation parameters should provide not only good accuracy but also a high temporal resolution, i.e., fast enough, to provide sufficient information of the flow. Electrical capacitance tomography (ECT) has been used for real-time measurement and analysis of gas-solid fluidized beds for many years because of its nonintrusive and noninvasive nature and high sampling rate [2]–[5]. In addition, it can provide not only cross-sectional, but also volumetric images by using a 3-D ECT sensor with multiplane electrodes [6]–[8].

For 3-D image reconstruction using a 3-D ECT sensor, capacitance signals should be measured between electrodes

Manuscript received February 1, 2021; revised March 21, 2021; accepted April 12, 2021. Date of publication April 22, 2021; date of current version May 6, 2021. This work was supported in part by the National Key Research and Development Program of China under Grant 2018YFB0604904 and in part by the National Natural Science Foundation of China under Grant 91834302. The Associate Editor coordinating the review process was Dr. Chao Tan. (Corresponding authors: Mao Ye; Shuanghe Meng.)

Jingjing Shen is with the National Engineering Laboratory for MTO, Dalian Institute of Chemical Physics, Chinese Academy of Sciences, Dalian 116023, China, and also with the University of Chinese Academy of Sciences, Beijing 100049, China (e-mail: shenjing@dicp.ac.cn).

Shuanghe Meng and Mao Ye are with the National Engineering Laboratory for MTO, Dalian Institute of Chemical Physics, Chinese Academy of Sciences, Dalian 116023, China (e-mail: mengshh@dicp.ac.cn; maoye@dicp.ac.cn).

Wuqiang Yang is with the Department of Electrical and Electronic Engineering, The University of Manchester, Manchester M13 9PL, U.K. (e-mail: w.yang@manchester.ac.uk).

This article has supplementary downloadable material available at https://doi.org/10.1109/TIM.2021.3075038, provided by the authors.

Digital Object Identifier 10.1109/TIM.2021.3075038

in different planes. One of the difficulties is that the measured signals between electrodes in planes far away from each other are very weak because of the long distance between the electrodes and complicated geometry, which are much smaller than that in the same or adjacent planes, and thus easily affected by noise [9], [10], [11]. It is estimated that the measured capacitance between electrodes in planes far away from each other is less than 1 femtoFarad (fF), which demands high sensitivity and high stability of the capacitance measuring circuit in an ECT hardware system [7], [12]. With such small capacitance, measurement errors present a big challenge [9]. Therefore, it is vital to improve the stability of the capacitance measuring circuit, so that the measurement errors can be reduced [13]. While the most direct way to reduce the measurement errors is to improve the hardware system [14], [15], it is difficult to do so because the cost of the equipment may be dramatically increased.

Because capacitance signals between electrodes in planes far away from each other are too small, some researchers simply neglect them [16]. Li and Holland [17] believed that the use of capacitance signals from electrodes in planes far away from each other provides little benefit to image reconstruction, and high-quality images can be obtained by using signals between electrodes in the same plane or a neighboring plane only. However, they obtained results by numerical simulation, and the influence of measurement errors on image quality was not considered. In addition, the quality of reconstructed images was not quantitatively analyzed. Because the number of voxels in a reconstructed image is much larger than that of measurement signals, the solution is seriously under-determined, making it difficult to obtain a good image [18], [19].

Because sensor design is very important for 3-D ECT, researchers have made tremendous effort on optimization of the 3-D ECT sensor design [20]. The design parameters for a 3-D ECT sensor include the number of electrodes in each plane, the length of electrodes, the number of electrode planes, and so on [9], [20]–[22]. An ECT sensor with hexagonal electrodes was preferred for providing less variation in sensitivity compared with rectangular electrodes [23]. Shen et al. [24] studied the effect of electrode arrangement and shape of 3-D ECT sensors on capacitance measurements and image quality, and the result showed that an ECT sensor with staggered hexagonal electrodes provides smaller measurement errors and higher image quality than rectangular electrodes. However, the area of electrodes mounted on the outside of a vessel or tube is limited, and hence the measured capacitance is limited.

1557-9662 © 2021 IEEE. Personal use is permitted, but republication/redistribution requires IEEE permission. See https://www.ieee.org/publications/rights/index.html for more information.

Multielectrode excitation, compared to single-electrode excitation, can provide enhanced magnitude for the detected capacitance signals, but it needs complicated excitation strategies in real measurements. Yang et al. [25] proposed an opposite multielectrode simultaneous asymmetric excitation for ECT with electrodes on a single plane, and the results show that it can significantly decrease the dynamic range of capacitance measurements and reduce the nonlinear effect on image reconstruction. Dual-electrode excitation is a more realistic choice in 3-D ECT measurement. But it is found that the dual-electrode excitation in the adjacent position and the same plane makes limited improvement to the capacitance measured for a 3-D ECT sensor with multiplane electrodes. Mao et al. [26] studied three different excitation strategies for an ECT sensor with three planes of rectangular electrodes with four electrodes in each plane by numerical simulations. The three excitation strategies include, single-electrode excitation, dual-electrode excitation in the same planes with adjacent positions, and dual-electrode excitation in the different planes with adjacent positions. They found that the reconstructed images of some static models by single-electrode excitation have better quality. Actually, Mao et al. [26] only conducted a numerical simulation study for simple static models, which can be considered as a preliminary work in terms of excitation strategy. Mao et al. [27] is an extension of their earlier work [26]. In this latter work, they added experiments with single static models. Differing from their earlier work [26], they showed that the minimum capacitance of dual-electrode excitation is apparently bigger than that of single-electrode excitation, and the uncertainty of capacitance measurements of dual-electrode excitation in different planes are superior to the other two excitation strategies. The work by Mao et al. [26], [27] can be considered as a preliminary work in terms of excitation strategy.

In this work, the performance of 3-D ECT sensors with several dual-electrode excitation is studied. The dual electrodes used for excitation are in the same plane, in adjacent planes, in planes separated by one plane or separated by two planes of the axial direction, and adjacent position and opposite position in the chosen planes. Three 3-D ECT sensors are investigated with different excitation strategies, including (1) three planes of rectangular electrodes with four electrodes in each plane, (2) four planes of rectangular electrodes with four electrodes in each plane, and (3) four planes of staggered hexagonal electrodes with four electrodes in each plane. The electric field distribution, sensitivity distribution, signal intensity, the disturbance of measurement signals, and the quality of reconstructed images of single static models, multiple static models, and moving models are analyzed for the 3-D ECT sensors with different excitation strategies.

# II. PROPOSED EXCITATION STRATEGIES

# A. ECT System

A 3-D ECT system is comprised of a multiplane capacitance sensor, a sensing electronics, and a computer for image reconstruction and processing, as shown in Supplementary Fig. S1. The ECT sensors detect the capacitance between the

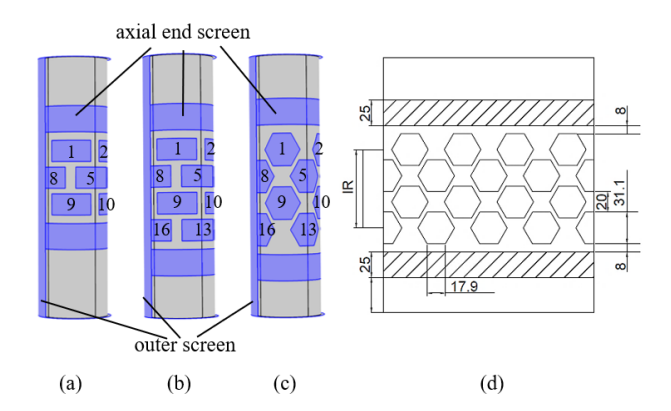


Fig. 1. 3-D ECT sensors. (a) S1, with three planes of rectangular electrodes and four electrodes in each plane. (b) S2, four planes of rectangular electrodes and four electrodes in each plane. (c) S3, four planes of staggered hexagonal electrodes and four electrodes in each plane. (d) Design parameters of S3. [unit: mm].

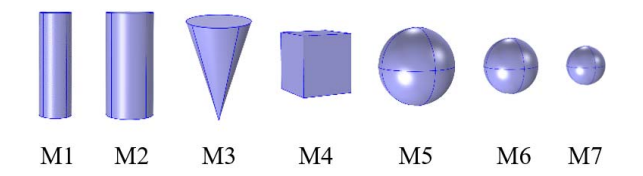


Fig. 2. Test models. (M1) cylinder: r=10 and h=60, (M2) cylinder: r=15 and h=60, (M3) cone: r=20 and h=60, (M4) cube: L=30, (M5) sphere: r=20, (M6) sphere: r=15, and (M7) sphere: r=10. [unit: mm].

excitation and detection electrodes, and the capacitance varies with the permittivity or permittivity distribution of materials. The capacitance is given by

$$C_{i,j} = -\frac{1}{V} \oint_{\Gamma} \varepsilon(x, y, z) \nabla \varphi(x, y, z) \cdot d\Gamma. \tag{1}$$

The normalized form of (1)

$$\lambda = Sg \tag{2}$$

where  $\lambda$ , S, and g are the normalized capacitance vector, normalized sensitivity matrix, and the normalized permittivity vector, respectively.

# B. Design of 3-D ECT Sensors

Fig. 1 shows the design of 3-D ECT sensors. Sensor 1 (S1) has 12 electrodes in three planes. Sensor 2 (S2) and Sensor 3 (S3) have 16 electrodes in four planes. Each sensor has two axial end screen electrodes and an outer screen electrode; these electrodes, which are earthed in the measurements, are used in preventing the influence of external noise signals in the measurements of the electrodes [28]. The materials used are listed in Table I.

All the electrodes are mounted outside a tube with an external diameter of 65 mm and wall thickness of 2.5 mm. Fig. 2 shows test models and their geometric parameters used in the experiment.

An automatic control system is used in this study, which is a closed loop system, mainly including a control panel, programmable logic controller, servo driver, servo motor, ball

TABLE I MATERIALS USED IN ECT SENSORS

Component	electrodes	tube	test models	high permittivity calibration	low permittivity calibration
Material	copper foil	glass	nylon	nylon	air
Permittivity	-	2	3	3	1

TABLE II DIFFERENT EXCITATION STRATEGIES FOR ECT SENSOR WITH MULTIPLANE ELECTRODES

Strateg ies	Excitation electrodes			
es11a	P1P1, P2P2: E1E2, E2E3, E3E4, E4E5, E5E6, E6E7, E7E8;			
	P3P3, P4P4: E9E10, E10E11, E11E12, E12E13, E13E14,			
	E14E15, E15E16.			
es12a	P1P2: E1E5, E5E2, E2E6, E6E3, E3E7, E7E4, E4E8;			
	P3P4: E9E13, E13E10, E10E14, E14E11, E11E15, E15E12,			
	E12E16.			
es12o	P1P2: E1E7, E7E2, E2E8, E8E3, E3E5, E5E4, E4E6;			
	P3P4: E9E15, E15E10, E10E16, E16E11, E11E13, E13E12,			
	E12E14.			
es13a	P1P3: E1E9, E9E2, E2E10, E10E3, E3E11, E11E4, E4E12;			
	P2P4: E5E13, E13E6, E6E14, E14E7, E7E15, E15E8, E8E16.			
es13o	P1P3: E1E11, E11E2, E2E12, E12E3, E3E9, E9E4, E4E10;			
	P2P4: E5E15, E15E6, E6E16, E16E7, E7E13, E13E8, E8E14.			
es14a	P1P4: E1E13, E13E2, E2E14, E14E3, E3E15, E15E4, E4E16;			
	P3P2: E9E5, E5E10, E10E6, E6E11, E11E7, E7E12, E12E8.			
es14o	P1P4: E1E15, E15E2, E2E16, E16E3, E3E13, E13E4, E4E16;			
	P3P2: E9E7, E7E10, E10E8, E8E11, E11E5, E5E12, E12E6.			

screw, and proximity sensor, as stated in [29]. In the experiment, we can precisely control the starting/ending position and moving velocity in the axial direction of the test model.

# C. Excitation Strategies

An ac-based ECT sensing electronics is used for measuring the capacitance between the electrodes [30]. Sine-wave voltage signals with amplitude of 20 V and frequency of 180 kHz are applied for electrodes excitation. Capacitance between the electrodes from different planes varies greatly because of different distances between the excitation electrodes and detection electrodes. Different dual-electrode excitation strategies are investigated. Table II gives the different excitation strategies for the ECT sensor, where a of the name of the strategy means that the two excitation electrodes are in the adjacent position, o means opposite position, "P1P2" means excitation electrodes are in the first and second planes, respectively. Adjacent dual-electrode excitation means the two electrodes used for excitation are adjacent. For example, taking electrode 1 as the excitation electrode, adjacent electrodes of electrode 1 are electrodes 2, 4, 5, 8, 9, 13, and 16, which have adjacent radial positions but different axial positions. And es11a with the excitation electrodes E1E2 is an excitation strategy of adjacent dual-electrode excitation, which also includes es12a,

es 13a, and es 14a. Opposite dual-electrode excitation means the two electrodes used for excitation are opposite. For example, opposite electrodes of electrode 1 are electrodes 3, 4, 6, 7, 11, 14, 15, and es120 with the excitation electrodes E1E7 is an excitation strategy of opposite dual-electrode excitation, which also includes es130 and es140.

Supplementary Fig. S2 shows the relative position of the dual-electrode excitation. Lines with arrows in Supplementary Fig. S2 link the dual-electrode in the adjacent position or opposite position used for excitation, e.g., electrodes 1 and 7 are used for simultaneous excitation in excitation strategy es12o, therefore electrodes 1 and 7 are linked by a line with an arrow. For distinguishing different dual-electrodes used for excitation, different arrows and colors are used for the excitation strategies if the arrows are interlaced or adjacent, and a single arrow with the same color is used if the arrows are clearly separated.

When an excitation strategy is applied, the dual-electrode shown in Table II are sequentially excited with a sinusoidal voltage signal, and meantime, the rest electrodes are used for detection. A group of two excitation electrodes and a detection electrode forms an electrode pair, and thus obtain a measuring signal for each measurement. Taking excitation strategy es12a as an example, electrodes 1 and 5 are first excited and the rest of the electrodes are used for detection and then electrodes 5 and 2 are excited and the rest of the electrodes are used for detection,..., until the electrodes 12 and 16 are excited and the rest of the electrodes are used for detection, which completes a group of measurements, and thus obtain a group of measuring signals. Therefore, a group of measurement contains 196 measuring signals.

# D. Image Reconstruction

Landweber iteration algorithm was used for image reconstruction, and the linear back-projection (LBP) was used to obtain the initial value of permittivity [29], [31], [32]. A median filter is used for processing artefacts and distortion of the reconstructed images [24].

# E. Evaluation Criteria

Image error (Ie) and correlation coefficient (Cc) are used for evaluating the quality of reconstructed 3-D images of test models, and the definition of Ie and Cc are, respectively,

$$Ie = \frac{\|\hat{g} - g\|}{\|g\|} \tag{3}$$

$$Cc = \frac{\sum_{i=1}^{N} (\hat{g}_i - \bar{\hat{g}})(g_i - \bar{g})}{\sqrt{\sum_{i=1}^{N} (\hat{g}_i - \bar{\hat{g}})^2 \sum_{i=1}^{N} (g_i - \bar{g})^2}}.$$
 (4)

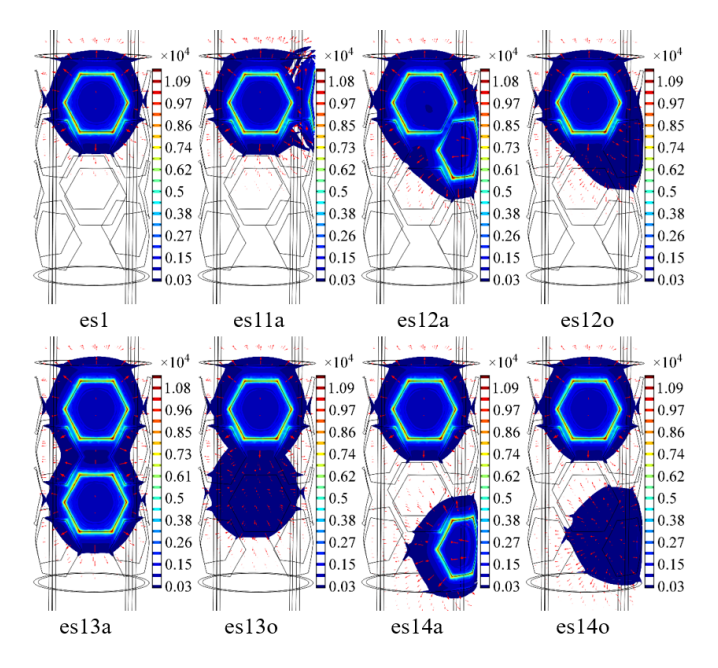


Fig. 3. Electric field distribution for ECT sensor with different excitation strategies.

### III. NUMERICAL SIMULATION

### A. Electric Field Distribution

Fig. 3 shows the electric field distribution with different excitation strategies, taking ECT sensor S3 as an example. The color bar of isosurface reflects the electric field intensity with the unit of V/m and linear coordinate. The length of red arrow represents the strength of electric field with logarithmic coordinate, which shows more distribution of small electric field intensity. For the excitation strategy es1 with single-electrode excitation in Fig. 3, the electric field decreases sharply in the axial direction with the increase in distance between the excitation electrode and the detection electrode in different planes, and the electric field intensity in the third and fourth planes is very small and almost invisible. This problem has little improvement for the excitation strategy es11a with dual-electrode excitation in adjacent position and same plane. When the position of dual-electrode excitation is in adjacent planes, with excitation strategies es12a and es12o, the electric field lines can be seen taking up most of the space near the excitation electrodes in the third plane. In addition, the distribution of electric field lines become more uniform when it occurs to excitation strategies es13a, es13o, es14a, and es14o. The increase in electric field intensity is favorable for the increase in capacitance, and thus excitation strategies es13a, es13o, es14a, and es14o are recommended for measurement.

### B. Capacitance Measurement

Fig. 4 shows comparison of mean capacitance and standard deviation (STD) for the 3-D ECT sensors with different excitation strategies, where capacitance is obtained by finite-element method (FEM) with COMSOL Multiphysics. A higher mean capacitance and a lower STD make it easy to measure

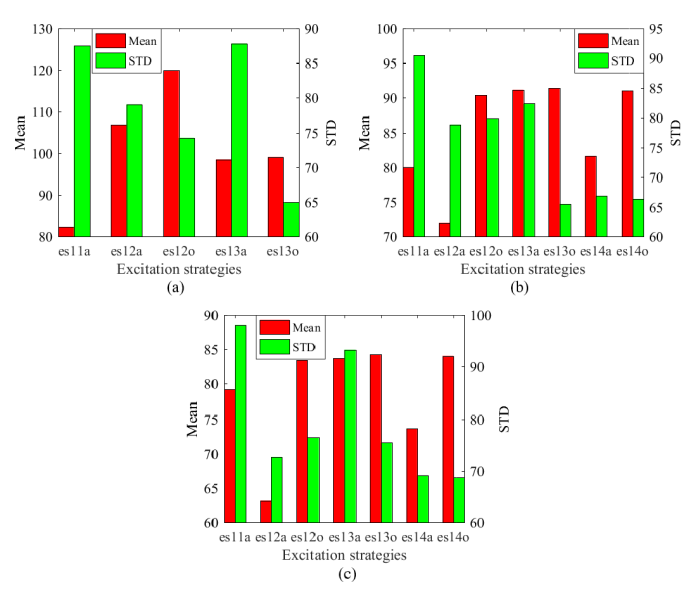


Fig. 4. Comparison of mean capacitance and STD of 3-D ECT sensors with different excitation strategies. (a) S1. (b) S2. and (c) S3.

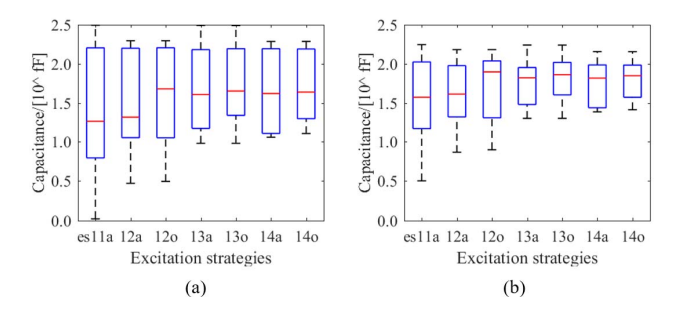


Fig. 5. Capacitance measurement for 3-D ECT sensor with different excitation strategies. (a) Range of capacitance when 3-D ECT sensor is filled with low-permittivity materials. (b) Dynamic range of capacitance measurement when 3-D ECT sensor is filled with high- and low-permittivity materials.

capacitance with small disturbance from noise. As shown in Fig. 4(a), for sensor S1, dual-electrode excitation in the opposite position provides higher mean capacitance and lower STD than in the adjacent position. For sensors S2 and S3, dual-electrode excitation in the opposite position provides higher mean capacitance but similar STD for excitation strategies es12 and es14, and lower STD of capacitance but similar mean capacitance for excitation strategy es13 than in the adjacent position. From the capacitance measurement point of view, dual-electrode excitation in the opposite position should be adopted.

A 3-D ECT sensor with four planes of electrodes can increase the number of independent capacitance measurement and the spatial resolution [1], [8], [33], [34]. Therefore, a 3-D ECT sensor S3 with four planes of staggered hexagonal electrodes was mainly discussed, which has good performance compared with the rectangular-shaped electrodes according to the measurement signals and image quality [24].

Fig. 5 shows the boxplot of capacitance measurements of sensor S3, and the value of capacitance was taken as the base-10 logarithm. The range of capacitance measurement

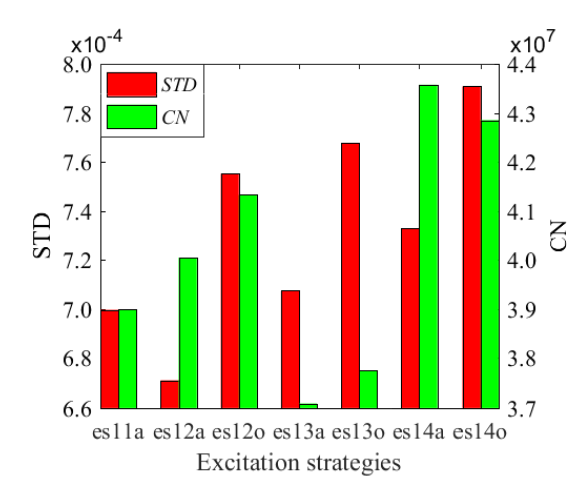


Fig. 6. Evaluation of sensitivity distribution for 3-D ECT sensor with different excitation strategies.

when the 3-D ECT sensor is filled with low-permittivity material is shown in Fig. 5(a). The dynamic range of capacitance measurement when the 3-D ECT sensor is filled with high-and low-permittivity materials is shown in Fig. 5(b).

The results confirm that different excitation strategies have great impact on the capacitance measurements, as discussed in Section III-A. The dynamic range of capacitance data obtained from the excitation strategies es13a, es13o, es14a, and es14o is remarkably less than the excitation strategy es11a, and the difference reaches to one order of magnitude because of the increase in small capacitance, especially for the minimum capacitance. For example, with excitation strategy es11a, the minimum capacitance of the 3-D ECT sensor is about 1 fF only, whereas it increases significantly to about 10 fF with excitation strategies es13a, es13o, es14a, and es14o. Even with dual-electrode excitation in adjacent planes, i.e., excitation strategies es12a and es12o, the minimum capacitance increases about two times. The maximum capacitance with different excitation strategies has no obvious difference. The increase in small capacitance and the decrease in dynamic range are beneficial to capacitance measurement.

### C. Sensitivity Field

COMSOL Multiphysics is used to compute the sensitivity distributions of a 3-D ECT sensor with different excitation strategies. For each excitation strategy, as introduced above, the dual-electrode shown in Table II are sequentially excited, and the rest of the electrodes are detected so that the electric field as well as sensitivity distribution can be calculated [35]. Fig. 6 shows the STD and condition number (CN) of normalized sensitivity distribution for a 3-D ECT sensor with different excitation strategies when the 3-D ECT sensor is filled with low-permittivity materials. STD and CN are defined in the following equations:

STD = 
$$\sqrt{\frac{1}{MN-1} \sum_{l=1}^{M} \sum_{k=1}^{N} (S_{l,k} - \bar{S})^2}$$
 (5)

$$CN = \sqrt{\frac{\lambda_1}{\lambda_n}}.$$
 (6)

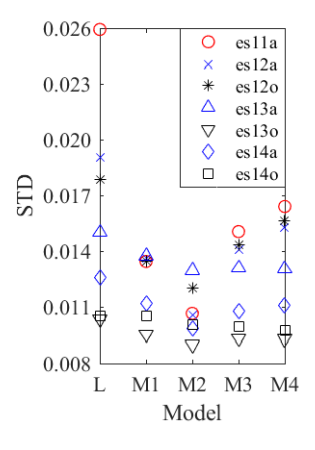


Fig. 7. Average STD of measurement signals with different test conditions for 3-D ECT sensor with different excitation strategies.

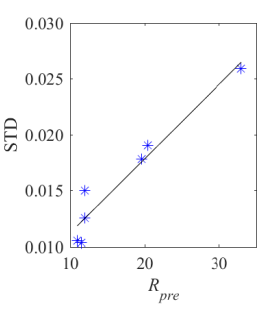


Fig. 8. Comparison of  $R_{pre}$  of capacitance data and STD of measured signals.

STD is used to evaluate the uniformity of the sensitivity distribution, with smaller STD representing more uniform distribution of sensitivity of voxels. CN indicates the ill-condition of image reconstruction, with smaller CN representing more robust image reconstruction of ECT. Therefore, it is important to reduce STD and CN in order to obtain high-quality reconstructed images [9]. Except for excitation strategy es12a, the uniformity of sensitivity distribution is decreased for the 3-D ECT sensor with dual-electrode excitation in different planes, compared with that within same plane of excitation strategy es11a. Dual-electrode excitation from the opposite position provides higher STD than that from the adjacent position. In addition, ill-condition in the image reconstruction process for the 3-D ECT sensor with excitation strategies es13a and es13o improves, compared with that with the excitation strategy es12a.

While there is no obvious variation or sudden changes in the sensitivity distribution in the axial direction, dead zones appear, causing difficulty in convergence in image reconstruction [17], [36]. Supplementary Fig. S3 shows the normalized sensitivity distribution in the axial direction of the 3-D ECT sensor S3 with different excitation strategies, confirming that there are no obvious dead zones for the 3-D ECT sensor.

The sensitivity in the central region is significantly less than that near the edge of an ECT sensor, causing low image quality [35], [37]. Therefore, the sensitivity in the central region is analyzed with excitation strategy es14o. Supplementary Fig. S4 shows the sensitivity of some voxels between different

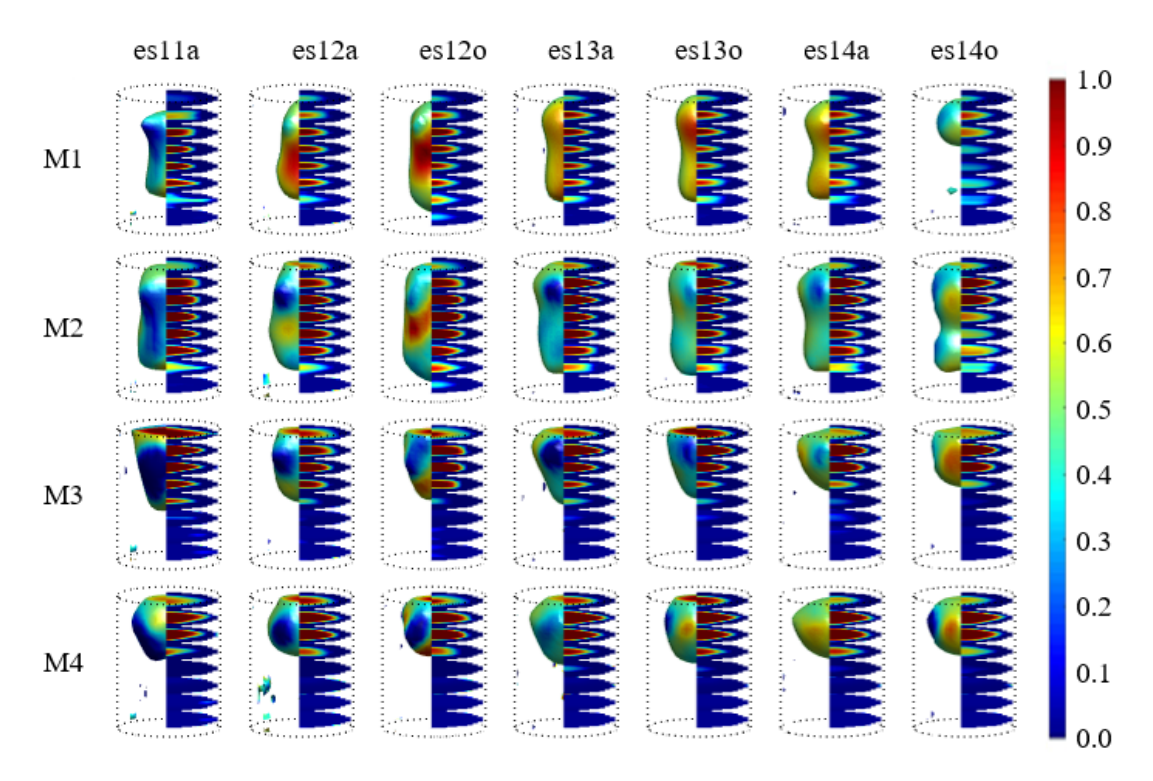


Fig. 9. Reconstructed images of different test models using 3-D ECT sensor with different excitation strategies.

electrode pairs of the 3-D ECT sensor S3, where the voxels in (a)–(g) are in the central region of x- and y-coordinates but different height (z-) coordinate, and that in (g)–(i) are in the same height (z-) and y-coordinates but different x-coordinate. The center of the bottom is defined as the coordinate origin (0, 0, 0).

When the height is less than 37.5 mm, with the increase in height of the voxels, the maximum sensitivity in the central region decreases and reaches to an order of magnitude when h = 37.5 mm, as shown in Supplementary Fig. S4(a)–(g). The total height in the axial direction is 76.8 mm, and it only shows the sensitivity of voxels with a height from 1.5 to 37.5 mm in Supplementary Fig. S4, because when the z-coordinate of voxels is larger than half of the total height, the sensitivity distribution has the opposite trend. It means that the voxel in the center region (x-, y-, and z-coordinates) is sensitive for none of the electrode pairs and hence is difficult to be measured. The closer the other voxels are to this voxel, it is less sensitive and more difficult to be measured. Therefore, the region near this voxel can be called sensitivity depression.

# IV. EXPERIMENT

# A. Measurement Signals

The disturbance of measurement signals in the experiment for a 3-D ECT sensor with different excitation strategies is compared as shown in Fig. 7, when the 3-D ECT sensor is filled with low-permittivity materials (L), and with different test models, i.e., M1, M2, M3, and M4. In this work, a total of 1000 groups of measurements were taken for each experiment. The STD is calculated using an electrode pair in 1000 groups of measurements, and average STD is

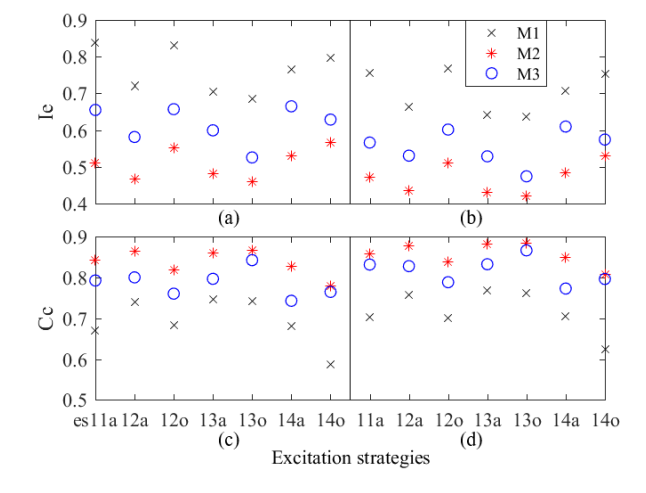


Fig. 10. Evaluation result of image quality of test models with different excitation strategies. (a) Ie without median filter. (b) Ie with median filter. (c) Cc without median filter. (d) Cc with median filter.

calculated by the average of STD of 196 electrode pairs. Because the difference of distance and relative position of electrode pairs, the quality and STD of measured signal are quite different. Therefore, average STD is defined here, which represents the total random errors of the measurement signals in each experiment condition. Measurement uncertainty is evaluated by the average STD. The STD with excitation strategies es12a and es12o is slightly decreased compared with excitation strategy es11a, whereas it has more meaningful decrease for other excitation strategies, like es13a, es13o, es14a, and es14o, especially for excitation strategy es13o, which confirms the result of the dynamic range of capacitance

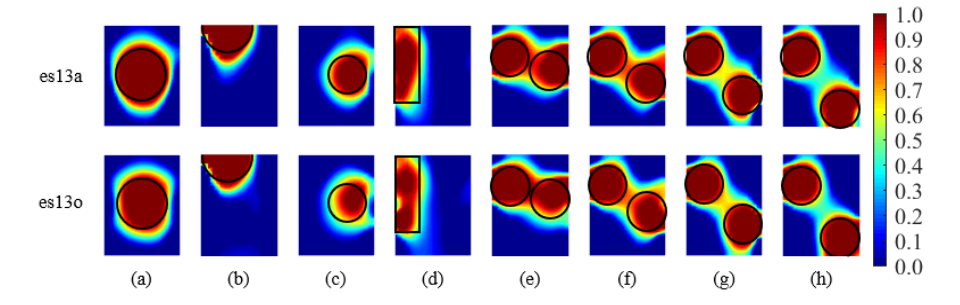


Fig. 11. Reconstructed images after median filter is applied with excitation strategies es 13a and es 13o. (a) M5. (b) Half of M5 in the top. (c) M6 close to the wall. (d) M1 contact the wall. From (e)–(h) are two M6 with different position.

in Fig. 5. If the signals were measured without the protection of the axial end screen electrodes and outer screen electrode, the STD of the signals would become larger owing to the effect of noises in the measurements.

There is a close relationship between simulation and experiment based on the above analysis. A factor  $R_{pre}$  in (7) is defined by the author to evaluate capacitance data obtained by numerical simulation

$$R_{\text{pre}} = \sum_{i=1}^{n} (1/c_i) \text{ [if } (1/c_i) < 0.05, \ (1/c_i) = 0.05].$$
 (7)

 $R_{\rm pre}$  represents the reverse of capacitance data between different electrode pairs, and the smaller the  $R_{\rm pre}$ , the larger the capacitance value. STD indicates random errors of measured signals, and the smaller the STD, the better the quality of measuring signals. In general, small capacitance value means small signal-to-noise ratio in the ECT measurements. Thus, there should be a positive correlation between  $R_{\rm pre}$  and STD of measuring signals. This is confirmed in Fig. 8, in which  $R_{\rm pre}$  shows to be almost linearly proportional to the STD of measuring signals. Other factors like the change in environment temperature and humidity, interference of electromagnetic signals, and static electricity are minor factors in this experiment.

### B. Image Reconstruction of Static models

Fig. 9 and Supplementary Fig. S5 show reconstructed images, which were obtained by use of 3-D ECT sensor S3, for different test models with different excitation strategies. Fig. 9 shows the original images and Supplementary Fig. S5 shows images processed using median filtering. All images are divided into two parts for better 3-D visualization. As can be seen, the quality of reconstructed images processed using median filter has been essentially improved as the artifacts in the original images were minimized in the processed images. The parameters used in the Landweber iteration include the relaxation factor  $\alpha = 5$  and iteration times of 500, based on the comprising between the quality of reconstructed images and calculation time. If choosing a smaller  $\alpha$  and iteration times, the apparent edge blur would appear, and if choosing a larger  $\alpha$  and iteration times, more computation time would be required. The left half is an isosurface image with a value of 0.5 and the right is a cross-sectional image after smooth interpolation. Most of the reconstructed images can show the main geometrical shapes of test models, but distortion occurs

obviously in the images of models M1 with excitation strategy es14o. The distortion was mainly observed in the center of sensing region. This might be due to the nonuniformity of the sensitivity distribution of 3-D ECT when the excitation strategy es14o was applied (as shown in Fig. 6) as well as the appearance of sensitivity depression in the center region (as shown in Supplementary Fig. S4).

Quantitative analysis of the quality of the image presented in Fig. 9 is conducted and the results are shown in Fig. 10. The image quality of test models with excitation strategies es12a, es13a, and es13o has higher Cc and lower Ie [38] than that with other excitation strategies. A median filter is used to process artifacts and distortion of reconstructed images and thus improve the image quality [24].

After the performance of the 3-D ECT sensor with different excitation strategies is comprehensively analyzed according to the capacitance measurement, sensitivity distribution, measurement signals, and image quality of some static models, the excitation strategy es130 is preferred. Some more complicated measurement conditions, including test models placed off-centered and multimodels, and the reconstructed images after the median filter are shown in Fig. 11.

Using the 3-D ECT sensor, the boundaries of a single test model in different positions and two test models placed with a certain distance can be distinguished. When the two models are placed near to each other, such as in Fig. 11(e) and (f), it is difficult to distinguish those two models because of the soft-field effect and low spatial resolution. In this case, further image processing may be used to obtain the boundaries of different test models. However, this work is focused on the performance of an ECT sensor with different excitation strategies, and image processing will be our future work.

### C. Image Reconstruction of Motion Models

For dynamic scenario involving the multiphase flows in a fluidized bed, the permittivity distribution of materials is changing over time, which makes the measurement more difficult. In addition, it is difficult to evaluate the image quality of a fluidized bed. Therefore, for further confirming the performance of 3-D ECT sensors with excitation strategy es130, experiment with motion models is conducted. The movements of models *M*5, *M*6, and *M*7 through the sensing region under different velocities (i.e., 100, 200, and 400 mm/s) have been investigated. All the models have been tested by

moving along the vertical axis through either the center or near the edge of the tube. The reconstructed 3-D ECT images for these models moving with different velocities and through different positions are shown in Figs. S6–S11. In the reconstructed images, 3-D ECT sensors with excitation strategy es130 can reconstruct the size and main shape of test models with different movement velocities and different positions. The reconstructed images of test models with movement further confirms the performance of 3-D ECT sensors with excitation strategy es130.

### V. CONCLUSION

In this article, the performance of 3-D ECT sensors with different dual-electrode excitation strategies, including es11a, es12a, es12o, es13a, es13o, es14a, and es14o, is studied. The effect of the spatial position of excitation electrodes on electric field distribution, capacitance measurement, sensitivity distribution, measurement signals, and image quality are evaluated. According to the obtained simulation and experimental results, the following conclusion can be drawn.

- 1) Dual-electrode excitation in the opposite position provides higher mean capacitance and lower STD than in the adjacent position. Dual-electrode excitation in different planes leads to an increase in capacitance and a reduction of the measurement range. Especially, the excitation strategies es13 and es14 improve the minimum capacitance between electrodes in the planes far away from each other by one order of magnitude, compared with that in the same plane. The improvement significantly reduces the demand for measuring equipment and is beneficial in decreasing the measurement uncertainty, which has been confirmed by experiment results of the STD of measured signals. The excitation strategy es130 has smaller signal disturbance than others.
- 2) The uniformity of sensitivity distribution is decreased with dual-electrode excitation in different planes compared with that within the same plane, but ill-condition in image reconstruction with excitation strategies es13a and es13o improves, compared with that with excitation strategy es11a. There exists a region for excitation strategy es14o where voxels have low sensitivity for all electrode pairs and are difficult to be measured.
- 3) The quality of the reconstructed images of some static models has been quantitatively analyzed, showing that the excitation strategies es12a, es13a, and es13o provide higher image quality than that with other excitation strategies.
- 4) After the performance of the 3-D ECT sensors with different excitation strategies is comprehensively analyzed, the excitation strategy es130 is recommended for further research for a 3-D ECT sensor with four planes of electrodes with four electrodes in each plane. The performance of 3-D ECT sensors with excitation strategy es130 is further confirmed by different static and motional test conditions.

The dual-electrode excitation strategies chosen in this study mainly involve the two excited electrodes in the adjacent and opposite positions. But we are well aware that there are indeed many other choices for excitation electrodes in 3-D ECT sensors in addition to those electrodes in adjacent or opposite positions. Besides dual-electrode excitation, the number of electrodes for excitation can also be 3 and more with number of electrodes for detection being 2 and more. Therefore, there are many combinations of the excitation and detection electrodes which deserve further investigation. It is of considerable interest to further optimize the combination of the excitation and detection electrodes under different measurement conditions, e.g., single static model, multiple static models, moving models, and the multiphase flows in fluidized beds. However, this is out of the scope of current work, and will be the topic of a future study concerning the complex excitation strategies of 3-D ECT sensors.

## REFERENCES

- [1] R. W. Breault, J. Weber, and L. J. Shadle, "The development of a generalized riser flow regime map based upon higher moment and chaotic statistics using electrical capacitance volume tomography (ECVT)," *Powder Technol.*, vol. 365, pp. 12–27, Apr. 2020.
- [2] T. Dyakowski, R. B. Edwards, C. G. Xie, and R. A. Williams, "Application of capacitance tomography to gas-solid flows," *Chem. Eng. Sci.*, vol. 52, no. 13, pp. 2099–2110, Jul. 1997.
- [3] T. C. Chandrasekera, Y. Li, D. Moody, M. A. Schnellmann, J. S. Dennis, and D. J. Holland, "Measurement of bubble sizes in fluidised beds using electrical capacitance tomography," *Chem. Eng. Sci.*, vol. 126, pp. 679–687, Apr. 2015.
- [4] K. Huang et al., "High-temperature electrical capacitance tomography for gas-solid fluidised beds," Meas. Sci. Technol., vol. 29, no. 10, Oct. 2018, Art. no. 104002.
- [5] S. Wang, X. Sun, C. Xu, J. Bao, C. Peng, and Z. Tang, "Investigation of a circulating turbulent fluidized bed with a fractal gas distributor by electrostatic-immune electrical capacitance tomography," *Powder Technol.*, vol. 361, pp. 562–570, Feb. 2020.
- [6] J. M. Weber and J. S. Mei, "Bubbling fluidized bed characterization using electrical capacitance volume tomography (ECVT)," *Powder Tech*nol., vol. 242, pp. 40–50, Jul. 2013.
- [7] D. Yang, L. Liu, and W. Feng, "Experimental investigation of an internally circulating fluidized bed with 32-electrode electrical capacitance volume tomography," *Measurement*, vol. 127, pp. 227–237, Oct. 2018.
- [8] A. Voss, P. Hosseini, M. Pour-Ghaz, M. Vauhkonen, and A. Seppänen, "Three-dimensional electrical capacitance tomography—A tool for characterizing moisture transport properties of cement-based materials," *Mater. Des.*, vol. 181, Nov. 2019, Art. no. 107967.
- [9] Y. Li and D. J. Holland, "Optimizing the geometry of three-dimensional electrical capacitance tomography sensors," *IEEE Sensors J.*, vol. 15, no. 3, pp. 1567–1574, Mar. 2015.
- [10] J. Zhao, X. Zou, W. Fu, and H. Zhang, "Fast adaptive electrical capacitance, volume tomography," in *Proc. 12th World Congr. Intell. Control Automat. (Wcica)*, Guilin, China, Jun. 2016, pp. 457–460.
- [11] Q. M. Marashdeh, F. L. Teixeira, and L.-S. Fan, "Adaptive electrical capacitance, volume tomography," *IEEE Sensors J.*, vol. 14, no. 4, pp. 1253–1259, Apr. 2014.
- [12] J. Kryszyn, D. Wanta, and W. T. Smolik, "Evaluation of the electrical capacitance tomography system for measurement using 3D sensor," *Informatyka, Automatyka, Pomiary Gospodarce Ochronie Rodowiska*, vol. 9, no. 4, pp. 52–59, Dec. 2019.
- [13] W. Q. Yang and T. A. York, "New AC-based capacitance tomography system," *IEE Proc.-Sci., Meas. Technol.*, vol. 146, no. 1, pp. 47–53, Jan. 1999.
- [14] D. Yang, C. Xu, B. Zhou, and S. Wang, "Small-diameter and high-pressure electrical capacitance tomography system based on PCI bus," *Chin. J. Sci. Instrum.*, vol. 28, no. 8, pp. 1399–1404, Aug. 2007.
- [15] S. Sun, L. Xu, Z. Cao, J. Sun, and W. Yang, "Signal demodulation methods for electrical tomography: A review," *IEEE Sensors J.*, vol. 19, no. 20, pp. 9026–9035, Oct. 2019.
- [16] R. K. Rasel, J. N. Sines, Q. Marashdeh, and F. L. Teixeira, "Cross-plane acquisitions in electrical capacitance volume tomography," *IEEE Sensors J.*, vol. 19, no. 19, pp. 8767–8774, Oct. 2019.

- [17] Y. Li and D. J. Holland, "Fast and robust 3D electrical capacitance tomography," *Meas. Sci. Technol.*, vol. 24, no. 10, Oct. 2013, Art. no. 105406.
- [18] Q. Marashdeh, L. S. Fan, B. Du, and W. Warsito, "Electrical capacitance tomography—A perspective," *Ind. Eng. Chem. Res.*, vol. 47, no. 10, pp. 3708–3719, May 2008.
- [19] P. Faia, R. Silva, M. G. Rasteiro, and F. Garcia, "Electrical tomography: A review of configurations, and application to fibre flow suspensions characterisation," *Appl. Sci.*, vol. 10, no. 7, Mar. 2020, Art. no. 2355.
- [20] M. Soleimani, H. Wang, Y. Li, and W. Yang, "A comparative study of 3D electrical capacitance tomography," *Int. J. Inf. Syst. Sci.*, vol. 3, no. 2, pp. 292–306, 2007.
- [21] J. Ye, H. Wang, and W. Yang, "Characterization of a multi-plane electrical capacitance tomography sensor with different numbers of electrodes," *Meas. Sci. Technol.*, vol. 27, no. 3, Mar. 2016, Art. no. 035103.
- [22] Z. Ye, H. Y. Wei, and M. Soleimani, "Resolution analysis using fully 3D electrical capacitive tomography," *Measurement*, vol. 61, pp. 270–279, Feb. 2015.
- [23] K. Brandisky, D. Sankowski, and R. Banasiak, "Analysis and simulation of novel hexagonal electrode electrical capacitance tomography sensor," in *Proc. IET 8th Int. Conf. Comput. Electromagn. (CEM)*, 2011, pp. 148–149, doi: 10.1049/cp.2011.0077.
- [24] J. Shen, S. Meng, J. Wang, W. Yang, and M. Ye, "Study on the shape of staggered electrodes for 3D electrical capacitance tomography sensors," *IEEE Trans. Instrum. Meas.*, vol. 1, 2020, Art. no. 4502110.
- [25] Y. Yang, L. Peng, and J. Jia, "A novel multi-electrode sensing strategy for electrical capacitance tomography with ultra-low dynamic range," *Flow Meas. Instrum.*, vol. 53, pp. 67–79, Mar. 2017.
- [26] M. Mao, J. Ye, H. Wang, J. Zhang, and W. Yang, "Excitation strategy for three-dimensional electrical capacitance tomography sensor," in *Proc. IEEE Int. Conf. Imag. Syst. Techn. (IST)*, Sep. 2015, pp. 49–54.
- [27] M. Mao, J. Ye, H. Wang, J. Zhang, and W. Yang, "Evaluation of excitation strategy with multi-plane electrical capacitance tomography sensor," *Meas. Sci. Technol.*, vol. 27, no. 11, Nov. 2016, Art. no. 114008.
- [28] W. Yang, "Design of electrical capacitance tomography sensors," Meas. Sci. Technol., vol. 21, no. 4, Apr. 2010, Art. no. 042001.
- [29] J. Shen, S. Meng, M. Ye, W. Yang, and Z. Liu, "3D image reconstruction using an ECT sensor with a single layer of electrodes," *Meas. Sci. Technol.*, vol. 31, no. 8, Aug. 2020, Art. no. 085106.
- [30] W. Q. Yang, "Further developments in an AC-based capacitance tomography system," Rev. Sci. Instrum., vol. 72, no. 10, pp. 3902–3907, Oct. 2001.
- [31] C. G. Xie et al., "Electrical capacitance tomography for flow imaging: System model for development of image reconstruction algorithms and design of primary sensors," *IEE Proc. G Circuits, Devices Syst.*, vol. 139, no. 1, pp. 89–98, Feb. 1992.
- [32] W. Q. Yang, D. M. Spink, T. A. York, and H. McCann, "An imagereconstruction algorithm based on Landweber's iteration method for electrical-capacitance tomography," *Meas. Sci. Technol.*, vol. 10, no. 11, pp. 1065–1069, 1999.
- [33] A. Wang, Q. M. Marashdeh, F. L. Teixeira, and L.-S. Fan, "Electrical capacitance volume tomography: A comparison between 12- and 24-channels sensor systems," *Prog. Electromagn. Res. M*, vol. 41, pp. 73–84, 2015, doi: 10.2528/PIERM15011412.
- [34] J. N. Sines et al., "Slurry bubble column measurements using advanced electrical capacitance volume tomography sensors," *Powder Technol.*, vol. 355, pp. 474–480, Oct. 2019.
- [35] P. N. Darma, M. R. Baidillah, M. W. Sifuna, and M. Takei, "Improvement of image reconstruction in electrical capacitance tomography (ECT) by sectorial sensitivity matrix using a K-means clustering algorithm," *Meas. Sci. Technol.*, vol. 30, no. 7, Jul. 2019, Art. no. 075402.
- [36] W. Warsito, Q. Marashdeh, and L.-S. Fan, "Electrical capacitance, volume tomography," *IEEE Sensors J.*, vol. 7, no. 4, pp. 525–535, Apr. 2007.
- [37] W. Q. Yang and W. F. Conway, "Measurement of sensitivity distributions of capacitance tomography sensors," *Rev. Sci. Instrum.*, vol. 69, no. 1, pp. 233–236, Jan. 1998.
- [38] W. Q. Yang and L. Peng, "Image reconstruction algorithms for electrical capacitance tomography," *Meas. Sci. Technol.*, vol. 14, no. 1, pp. R1–R13, Jan. 2003.



Jingjing Shen received the B.Eng. degree from Zhengzhou University, Zhengzhou, China, in 2016. He is working toward the Ph.D. degree with the Dalian Institute of Chemical Physics, Chinese Academy of Sciences, Dalian, China, and also with the University of Chinese Academy of Sciences, Beijing, China.

He conducts academic research about multiphase flow measurement and simulation based on 3-D electrical capacitance tomography (ECT) technology.



**Shuanghe Meng** received the B.Eng. degree from the Dalian University of Technology, Dalian, China, in 1984

From 1984 to 1986, she was an Assistant Engineer with the Dandong Ray Instrument Industry Corporation, Dandong, China. She became an Assistant Engineer in 1986 and an Engineer in 1989 with the Dalian Institute of Chemical Physics, Dalian, where she has been a Senior Engineer since 1999. Her research interests include ECT technology and its application in industry and thermochemistry.



**Wuqiang Yang** (Fellow, IEEE) received the B.Eng., M.Sc., and Ph.D. degrees from Tsinghua University, Beijing, China, in 1982, 1985, and 1988, respectively.

After three years as a Lecturer at Tsinghua University, he joined the University of Manchester Institute of Science and Technology (UMIST) (now The University of Manchester), Manchester, U.K., in 1991, where he has been a Professor of electronic instrumentation since 2005. He has authored or coauthored 400 articles and edited two books: *Sensor Array* and

*Imaging Sensor Technologies and Applications*. He has been invited by many universities, research institutions, companies, and international conferences worldwide to give lectures, seminars, and keynotes. His research interest is electrical capacitance tomography (ECT) and its industrial applications.

Dr. Yang is a fellow of the IET and the Institute of Measurement and Control and CEng (U.K.). He is currently an Associate Editor of the IEEE TRANSACTIONS ON INSTRUMENTATION AND MEASUREMENT and the IET Science Measurement and Technology, an Editorial Board Member of six other journals, including Measurement of Science and Technology, and a Guest Editor of more than ten journal special issues. He was an IEEE IMS Distinguished Lecturer from 2010 to 2016. Since 2002, he has been in Who's Who in the World.



Mao Ye received the B.Eng. degree from the Jiangsu University of Science and Technology, Zhenjiang, China, in 1994, and the M.Eng. and Ph.D. degrees from Southeast University, Nanjing, China, in 1997 and 2000, respectively.

Since 2010, he has been a Professor of chemical engineering with the Dalian Institute of Chemical Physics, Chinese Academy of Sciences, Beijing, China. His current research interests include multiphase catalytic processes, measurement and simulation of multiphase flows, and industrial fluidized bed reactors.